Eulerian Simulation Strategy for Scaling up a Bubble Column Slurry Reactor for Fischer−Tropsch Synthesis

J. M. van Baten and R. Krishna*

Department of Chemical Engineering, University of Amsterdam, Nieuwe Achtergracht 166, 1018 WV Amsterdam, The Netherlands

CFD simulations were carried out in the Eulerian framework using both two-dimensional (2D) axisymmetric and transient three-dimensional (3D) strategies to describe the influence of column diameter on the hydrodynamics and dispersion characteristics of the bubble column slurry reactor for Fischer−Tropsch (FT) synthesis. Interactions between the bubbles and the slurry were taken into account by means of a momentum-exchange, or drag, coefficient; this coefficient was estimated from experimental data on the bubble swarm velocity in the limit of low superficial gas velocity U. The turbulence in the slurry phase was described using the $k-\epsilon$ model. For an FT slurry reactor operating at $U = 0.15$ m/s, simulations were also carried out for columns with diameters of 0.38, 1, 2, 4, 6, and 10 m using the 3D simulation strategy to determine gas hold-up; the liquid circulation velocity; and the axial dispersion coefficient of the liquid phase, $D_{ax,L}$. The results demonstrate the strong increase of liquid circulation and $D_{ax,L}$ with increasing column diameter. We conclude that 3D Eulerian simulations can provide a powerful tool for hydrodynamic scale-up of bubble columns, obviating the need for large-scale experiments.

Introduction

The Fischer−Tropsch (FT) reaction, which was discovered in Germany nearly three-quarters of a century ago, has recently become a subject of renewed interest particularly in the context of the conversion of remote natural gas to liquid transportation fuels. For economic and logistics reasons, such conversions are best carried out in large-scale projects, so the capability of upscaling is an important consideration in the selection of reactors for synthesis gas generation, as well as for FT synthesis. It is now widely accepted that the bubble column slurry reactor is the best choice of reactor type for large-scale plants with capacities on the order of 40 000 bbl/day of liquid hydrocarbon product.[1,2] Typical design and operating conditions of an FT slurry bubble column reactor are as follows:[3,4] diameter $D_T = 6-10$ m, height $H_T = 30-40$ m, operating pressure $= 3-4$ MPa, and temperature $T = 513-523$ K. The superficial gas velocity U is in the range 0.1−0.3 m/s depending the catalyst activity and the catalyst concentration in the slurry phase.[3] For high reactor productivities, the highest slurry concentrations consistent with catalyst handleability should be used. In practice, the volume fraction of catalyst in the slurry phase, ϵ_s, is in the range of 0.2−0.4. For removing the heat of reaction, 5000−8000 vertical cooling tubes, say, of 50-mm diameter and 150-mm pitch, will need to be installed in a reactor of, say, 6-m diameter. Most, if not all, of the mentioned features of the FT reactor represent major departures from typical reactor technology, requiring a careful and systematic approach to scale-up.

The economic success of the FT process largely depends on the ability to achieve deep syngas conversions, say, exceeding 95%. Reliable design of the reactor to achieve such high conversion levels requires reasonably accurate information on the following hydrodynamics and mass-transfer parameters: gas hold-up, ϵ; volumetric mass-transfer coefficient, k_La; heat-transfer coefficient to the cooling tubes, α; and axial dispersion coefficients of the liquid (slurry) and gas phases, $D_{ax,L}$ and $D_{ax,G}$, respectively. Most of the above-mentioned hydrodynamic parameters are interrelated.

Let us first consider the issue of estimating ϵ. The influence of the solids concentration, ϵ_s, on ϵ, according to published data,[5] is shown in Figure 1a for a 0.38-m-diameter column with paraffin oil as the liquid phase and silica catalyst particles as the solids. It is observed that an increased particle concentration tends to decrease the total gas hold-up, ϵ, significantly. This decrease in the total gas hold-up is due to the decrease in the hold-up of the small bubbles due to enhanced coalescence caused by the presence of the small catalyst particles. At low solid concentrations, there is a pronounced maximum in the gas hold-up, which is typical of the transition from a homogeneous to a heterogeneous flow regime.[4] With an increased solids concentration, the transition occurs at a lower superficial gas velocity, and the window of operation in the homogeneous regime becomes narrower. At catalyst particle concentrations exceeding 30 vol %, the dispersion consists almost exclusively of fast-rising large bubbles belonging to the spherical cap family. The gas hold-up in concentrated slurries has been shown to have almost the same value as the gas hold-up in a highly viscous liquid,[5] such as Tellus oil with a viscosity of 75 mPa s. Furthermore, dynamic gas disengagement experiments[5] have established that, for both Tellus oil and concentrated paraffin oil slurries, the gas dispersion consists predominantly of large bubbles. Tellus oil can therefore be used to mimic the hydroydnamics of an FT reactor with concentrated slurries. A recent experimental study by Urseanu et al.[6] has shown that the influence of operating pressure on the gas hold-up is negligible for high-viscosity liquids, and therefore, we can conclude that the experimental gas hold-ups for Tellus oil at atmospheric conditions are representative of those of an FT reactor that operates at 3−4 MPa.

Figure 1b shows the influence of the column diameter, D_T, on ϵ for an oil slurry with $\epsilon_s = 0.36$; we see that the

* To whom correspondence should be addressed. Fax: +31 205255604. Tel: +31 205257007. E-mail: krishna@science.uva.nl

10.1021/ie0340286 CCC: $27.50
Published on Web 11/25/2003

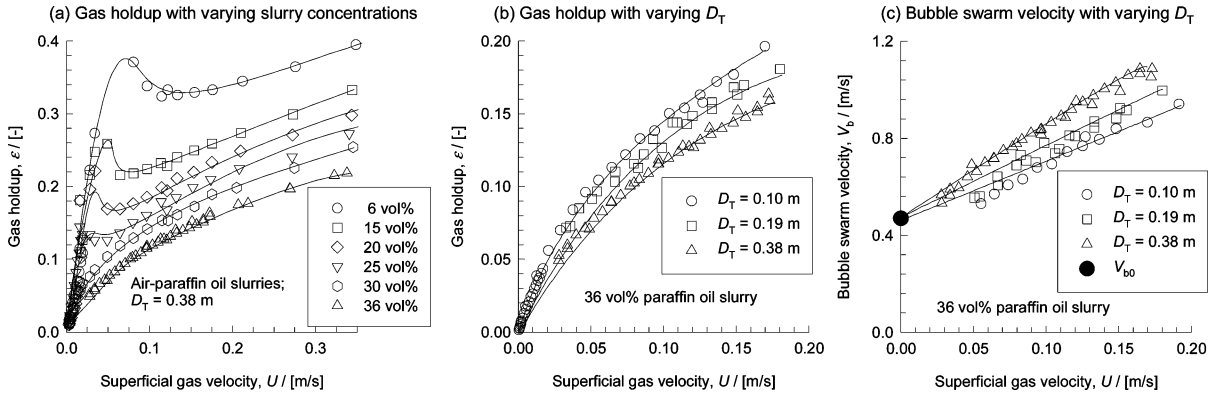

Figure 1. (a) Influence of concentration of catalyst particles ϵ_s on the gas hold-up ϵ in a 0.38-m-diameter column. (b) Influence of column diameter D_T on ϵ for a paraffin oil slurry with $\epsilon_s = 0.36$. (c) Influence of D_T on the average bubble swarm velocity for a paraffin oil slurry with $\epsilon_s = 0.36$. Also plotted are the experimental data of Krishna et al.[5]

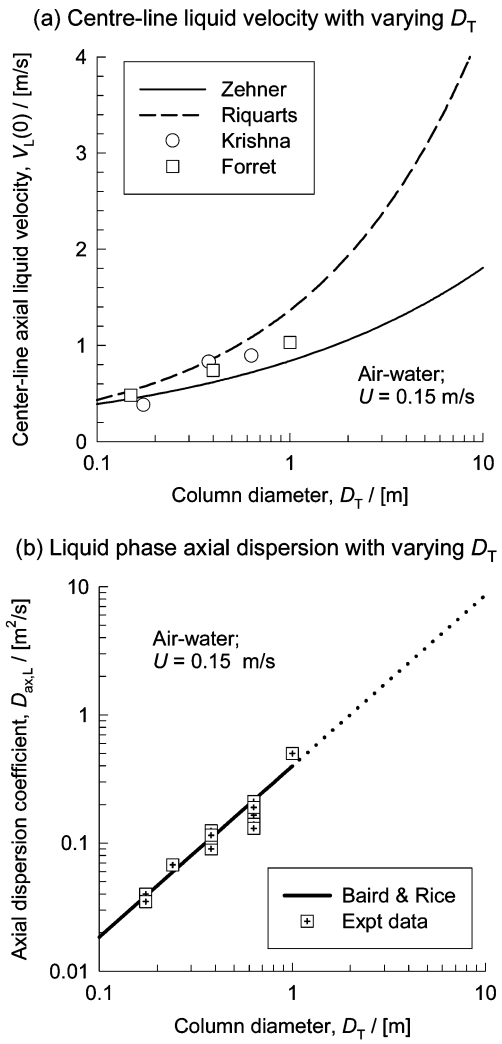

Figure 2. (a) Centerline liquid velocity $V_L(0)$ for air−water bubble columns as a function of column diameter D_T. (b) Liquid-phase axial dispersion coefficient $D_{ax,L}$ for air−water bubble columns as a function of column diameter D_T. Also plotted are the experimental data of Forret et al.[8] and Krishna et al.[11]

gas hold-up decreases with increasing D_T. An exactly analogous dependence of ϵ on D_T has been observed for the highly viscous Tellus oil.[5,7] With increasing column diameter, the liquid (slurry) circulation velocities are higher, and consequently, the bubbles tend to be accelerated, leading to lower gas hold-ups. This is evidenced by plotting the bubble swarm velocity, V_b, calculated from $V_b = U/\epsilon$, for the three column diameter values $D_T = 0.1$, 0.19, and 0.38 m; see Figure 1c. For the vanishingly small U, the bubble swarm velocity is practically the same for the three columns, and $V_{b0} = 0.47$ m/s; this is indicated by the large filled circle in Figure 1c. Below, we shall use the value $V_{b0} = 0.47$ m/s to determine the drag coefficient between the large bubbles and the liquid and thereby "calibrate" the CFD simulations.

In contrast to the results shown in Figure 1, published experimental work on *air−water* systems[8,9] show that the influence of column diameter on the *total* gas hold-up is negligible. The rationalization of these observations is as follows: For air−water systems, there is essentially a bimodal bubble size distribution, with "small" and "large" bubble size populations.[4] With increased liquid circulation, the large bubbles that are concentrated in the central core tend to rise faster, and there is a decrease in the large bubble gas hold-up. The small bubbles, however, are predominantly present in the peripheral wall region;[10] with increased liquid circulation, the small bubbles are dragged downward in the wall region, and this leads to *higher* small bubble hold-up with increased column diameter. The *total* gas hold-up is virtually unaltered with increasing column diameter. The situation with Tellus oil and concentrated slurries is quite different. In this case, the hold-up consists predominantly of large bubbles,[5] and therefore, increased liquid circulation leads to a decrease in the total gas hold-up.

The liquid circulation tends to accelerate the bubbles traveling upward in the central core. When the bubbles disengage at the top of the dispersion, the liquid travels back down the wall region. Clearly, to describe the influence of liquid circulation on the gas hold-up, we need to be able to predict the liquid circulation velocity as a function of U and D_T. One measure of the liquid circulation is the velocity of the liquid at the central axis of the column, $V_L(0)$. Figure 2a shows published data of Forret[8] and Krishna[11] on $V_L(0)$ for air−water systems for D_T in the range 0.1−1 m. Also shown in Figure 2a are the literature correlations for $V_L(0)$ of Riquarts[12]

$$V_L(0) = 0.21(gD_T)^{1/2}(U^3\rho_L/g\mu_L)^{1/8} \quad (1)$$

and Zehner[13]

$$V_L(0) = 0.737(UgD_T)^{1/3} \quad (2)$$

The major uncertainty in extrapolating to, say, $D_T = 10$ m, for the FT reactor operating with concentrated oil slurries is self-evident, especially in view of the fact

that no experimental data are available for columns larger than 1 m in diameter. In this connection, it must be remarked that the experimental work of Koide[14] and Kojima,[15] carried out in a 5.5-m-diameter column, can not be used for our purposes because the operation was restricted to superficial gas velocities below 0.05 m/s.

With increasing liquid circulation, the dispersion (backmixing) in the liquid phase increases. For the FT reactor, the requirements conflict. To prevent hot spots and runaways, one would like a state of well-mixedness. However, from the point of view of achieving high syngas conversions, one would like to have more staging of the liquid phase.[16] In any event, a good estimation of the axial dispersion coefficient of the liquid phase, $D_{ax,L}$, is vitally important. Figure 2b shows measured data[8,17] on $D_{ax,L}$ for the air−water system for D_T in the range of 0.1−1 m. Also shown in Figure 2b is the Baird and Rice[18] correlation for $D_{ax,L}$

$$D_{ax,L} = 0.35 D_T^{4/3} (gU)^{1/3} \tag{3}$$

The applicability of the Baird−Rice correlation for estimation of $D_{ax,L}$ for a 10-m-diameter FT reactor operating with concentrated oil slurries is open to question, as the database used for setting up the correlation consisted largely of data from air−water experiments in columns smaller than 1 m in diameter, operating at atmospheric pressure. The influence of the operating pressure on $D_{ax,L}$ has been investigated by Wilkinson[19] and Yang and Fan;[20] their results, however, are contradictory. Whereas Wilkinson[19] reported an increase of $D_{ax,L}$ with increasing pressure, Yang and Fan[20] reported a decrease of $D_{ax,L}$ with increasing pressure. In any event, the effect of pressure on $D_{ax,L}$ can be expected to be small.

The major objective of the present work is to develop a strategy for obtaining information on the gas holdup, liquid circulation, and liquid dispersion for column dimensions and operating conditions relevant to the FT commercial reactor. Our approach relies on the use of computational fluid dynamics (CFD) in the Eulerian framework, using both two-dimensional (2D) axisymmetric and three-dimensional (3D) strategies. First, we establish the ability of CFD simulations to reproduce the scale dependence portrayed in Figure 1 for a concentrated oil-slurry system ($\epsilon_s = 0.36$) in columns with diameters of 0.1, 0.19, and 0.38 m, using both 2D and 3D simulations. In the second campaign, we use 3D simulations for columns with diameters of 0.38, 1, 2, 4, 6, and 10 m to establish the influence of D_T on ϵ, $V_L(0)$, and $D_{ax,L}$. For the latter campaign with varying D_T, the aspect ratios of the various columns were maintained above 5.

2. Development of Eulerian Simulation Model

For either gas or liquid phase, the volume-averaged mass and momentum conservation equations in the Eulerian framework are given by

$$\frac{\partial(\epsilon_k \rho_k)}{\partial t} + \nabla\cdot(\rho_k \epsilon_k \mathbf{u}_k) = 0 \tag{4}$$

$$\frac{\partial(\rho_k \epsilon_k \mathbf{u}_k)}{\partial t} + \nabla\cdot(\rho_k \epsilon_k \mathbf{u}_k \mathbf{u}_k) = \mu_{k,\mathrm{eff}} \epsilon_k [\nabla \mathbf{u}_k + (\nabla \mathbf{u}_k)^T] - \epsilon_k \nabla p + \mathbf{M}_{k,l} + \rho_k \epsilon_k \mathbf{g} \tag{5}$$

where ρ_k, $\mathbf{u}_k$, and ϵ_k represent, respectively, the macroscopic density, velocity, and volume fraction of phase k; $\mu_{k,\mathrm{eff}}$ is the effective viscosity of the fluid phase k, including the molecular and turbulent contributions; p is the pressure; $\mathbf{M}_{k,l}$ is the interphase momentum exchange between phase k and phase l; and $\mathbf{g}$ is the gravitational force. On the basis of the established hydrodynamic similarities between bubble columns operating with concentrated slurries ($\epsilon_s > 0.3$) and highly viscous liquids,[5] we treat the slurry phase as a highly viscous liquid phase and use the properties of Tellus oil ($\rho_L = 862$, $\mu_L = 0.075$, $\sigma = 0.028$).

The momentum exchange between the gas phase (subscript G) and liquid phase (subscript L) is given by

$$\mathbf{M}_{L,G} = \left[\frac{3}{4}\frac{C_D}{d_b}\rho_L\right]\epsilon_G \epsilon_L (\mathbf{u}_G - \mathbf{u}_L)|\mathbf{u}_G - \mathbf{u}_L| \tag{6}$$

where we follow the formulation given by Pan et al.[21] We have included only the drag force contribution to $\mathbf{M}_{L,G}$, in keeping with the works of Sanyal et al.[22] and Sokolichin and Eigenberger.[23] The added mass and lift force contributions were both ignored in the present analysis. For a bubble swarm rising in a gravitational field, the drag force balances the differences between the weight and buoyancy, and so the square-bracketed term in eq 6 containing the drag coefficient C_D becomes[24]

$$\frac{3}{4}\frac{C_D}{d_b}\rho_L = (\rho_L - \rho_G) g \frac{1}{V_{b0}^2} \tag{7}$$

where V_{b0} is the rise velocity of the bubble swarm in the limit of vanishing superficial gas velocity (as indicated by the large filled circle in Figure 1c); $V_{b0} = 0.47$ m/s. The choice of $V_{b0} = 0.47$ m/s serves to calibrate the CFD simulations and can be regarded as a fit parameter. When the superficial gas velocity U is increased, liquid circulation tends to "kick in", and eq 6 will properly take account of the slip between the gas and liquid phases. Our approach is valid when the bubble size does not increase significantly with increasing U. Measurements of the mass transfer in slurries[25] show that $k_L a/\epsilon$ is practically independent of U, and this underlines the correctness of the assumption of a constant bubble size. It is important to stress that we do not need to know the bubble diameter d_b to calculate the momentum exchange $\mathbf{M}_{L,G}$.

For the continuous, liquid (slurry) phase, the turbulent contribution to the stress tensor is evaluated by means of the $k-\epsilon$ model using standard single-phase parameters $C_\mu = 0.09$, $C_{1\epsilon} = 1.44$, $C_{2\epsilon} = 1.92$, $\sigma_k = 1$, and $\sigma_\epsilon = 1.3$. The applicability of the $k-\epsilon$ model has been considered in detail by Sokolichin and Eigenberger.[23] No turbulence model is used for calculating the velocity fields inside the dispersed bubble phases.

A commercial CFD package, CFX 4.4, by AEA Technology, Harwell, U.K., was used to solve the equations of continuity and momentum. This package is a finite-volume solver, using body-fitted grids. The grids are nonstaggered, and all variables are evaluated at the cell centers. An improved version of the Rhie−Chow algorithm[26] is used to calculate the velocity at the cell faces. The pressure−velocity coupling is obtained using the SIMPLEC algorithm.[27] For the convective terms in eqs 4 and 5, hybrid differencing was used. A fully implicit backward-differencing scheme was used for the time integration.

A pressure boundary condition was applied to the top of the column. A standard no-slip boundary condition

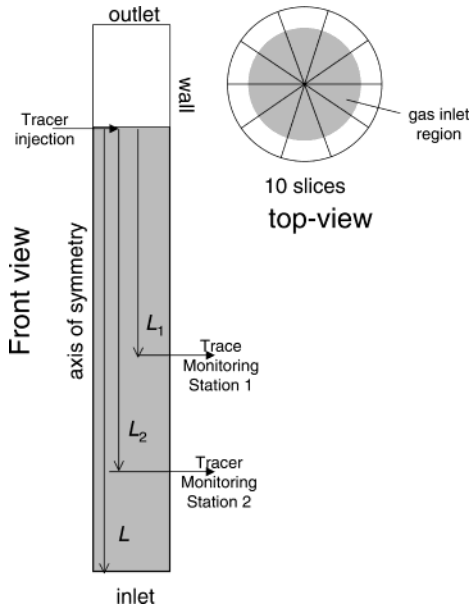

Figure 3. Schematic showing the computational domain and the tracer injection and monitoring stations to determine $D_{ax,L}$.

Table 1. Physical Properties of Phases Used in CFD Simulations

	liquid (Tellus oil)	gas (air)
viscosity, μ (Pa s)	75×10^{-3}	1.7×10^{-5}
density, ρ (kg/m^3)	862	1.3
diffusivity of tracer, $\mathscr{D}$ (m^2/s)	1×10^{-9}	–

was applied at the wall. The physical properties of the gas and liquid phases are specified in Table 1. The details of the operating conditions and computational grids used in the various campaigns are specified in Table 2. For any simulation, the column was filled with liquid to a certain height (as specified in Table 2), and at time zero, the gas velocity was set at the final value at the bottom face. For 2D simulations, to prevent a circulation pattern in which the liquid flows up near the wall and comes down in the core, the gas was not injected homogeneously over the full bottom area. Instead, the injection of gas was performed on the inner 75% of the radius. The choice of aeration of 75% of the central core at the bottom is arbitrary, but the results are only slightly different (within 10%) than if the gas injection had been taken to be 50% of the central distributor region. The gas aeration strategy is not very critical to the results of 3D transient simulations, as the flow is chaotic and the dispersion swishes from side to side.

The typical time-stepping strategy used was as follows: 100 steps at 5×10^{-5} s, 100 steps at 1×10^{-4} s, 100 steps at 5×10^{-4} s, 100 steps at 1×10^{-3} s, 200 steps at 3×10^{-3} s, 1400 steps at 5×10^{-3} s, and all remaining steps at 1×10^{-2} s until real (in the case of 2D) or quasi- (in the case of 3D) steady state was obtained. Quasi-steady state in 3D simulations was indicated by a situation in which each variable varied around a constant average value for a sufficiently long time period. In 2D simulations, true steady state was obtained in which none of the variables was subject to change.

To estimate the liquid-phase axial dispersion, the final state of a hydrodynamics run was used to start a dynamic run in which a mass tracer was injected into the liquid phase near the top of the dispersion. The concentration of the mass tracer was monitored at two heights along the column, following a simulation technique described in an earlier work.[10] The following equations are solved for the mass tracer

$$\frac{\partial}{\partial t}\epsilon_k \rho_k C_k + \nabla\cdot(\epsilon_k \rho_k \mathbf{u}_k C_k - \mathscr{D}_k \epsilon_k \rho \nabla C_k) = 0 \qquad (8)$$

Here, C_k is the concentration of mass tracer in phase k, and $\mathscr{D}_k$ is the diffusion coefficient of mass tracer in phase k (listed in Table 1). Because there is zero liquid throughput (liquid operates in batch), eventually all of the mass tracer gets distributed equally along the liquid phase. For the mass tracer simulations, some smaller time steps were used to guarantee a smooth restart from the hydrodynamics run, and then time steps of 5×10^{-3} s were used for the 0.38-m-diameter column, and time steps of 1×10^{-2} s were used for all remaining column diameters.

The liquid-phase axial dispersion coefficient was determined by a least-squares fit of the liquid-phase RTD curves at a distance L_i from the point of tracer injection[28]

$$\frac{C_L(x,t)}{C_{L,0}} = 1 + 2\sum_{n=1}^{\infty} \cos\left(\frac{n\pi L_i}{L}\right) \exp\left[-D_{ax,L}\left(\frac{\pi n}{L}\right)^2 t\right] \qquad i = 1, 2, 3 \quad (9)$$

Table 2. Details of 2D and 3D Simulation Campaign

campaign	column diameter, D_T (m)	gas velocity, U (m/s)	column height, H_T (m)	observation height for hydrodynamics, H_{obs} (m)	initial height of liquid in the column, H_0 (m)	cells in radius	cells in height	cells in azimuthal direction	total number of cells	number of days to complete hydrodynamics and RTD[a] (each run)
2D	0.1, 0.19, 0.38	0.02, 0.05, 0.1, 0.15	1.3	0.9	0.9–1	20	130	–	2600	1
3D	0.38	0.02, 0.05, 0.1, 0.15, 0.2, 0.23	1.3	0.9	0.9	20	130	10	26 000	5
3D	0.38	0.15	2.66	1.52	1.76	15	133	10	19 950	5
	1.0	0.15	7.0	4.5	4.65	20	140	10	28 000	9
	2.0	0.15	14.0	6.0	9.3	30	210	10	63 000	16
	4.0	0.15	28.0	14.4	18.64	40	350	10	140 000	44
	6.0	0.15	42.0	24.0	28.0	50	420	10	210 000	65
	10.0	0.15	42.0	24.0	28.0	50	420	10	210 000	65

[a] The RTD campaign was carried out only for the 3D simulations. Note that, for the 0.38-m-diameter column, two sets of 3D simulations were carried out; these sets differed in their aspect ratio. When comparing the hydrodynamics of columns of diameters in the 0.38–10-m range, the simulation results obtained with the higher aspect ratio was used.

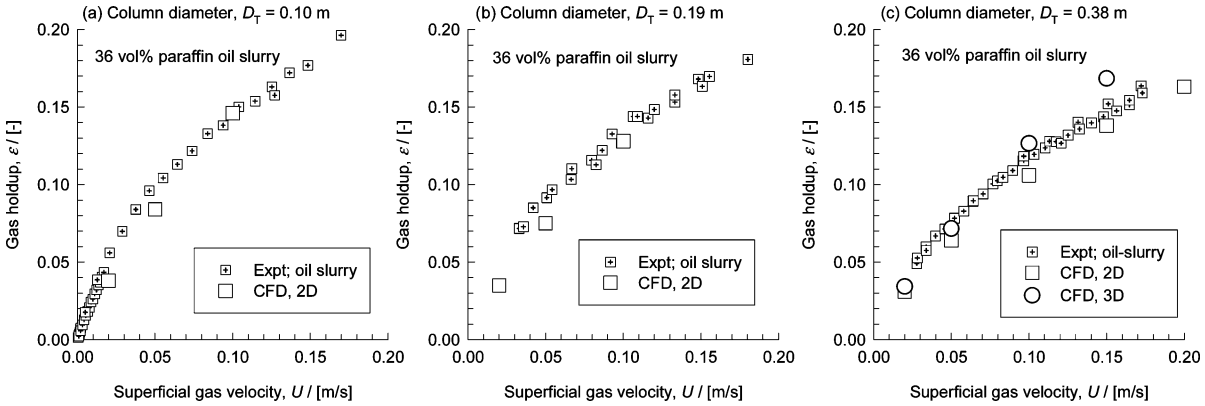

Figure 4. Data on gas hold-up as a function of the superficial gas velocity U for columns of diameters D_T = 0.1, 0.19, and 0.38 m for a 36 vol % paraffin oil system. Comparison with CFD simulations, both 2D axisymmetric and 3D, with experimental data of Krishna et al..[5]

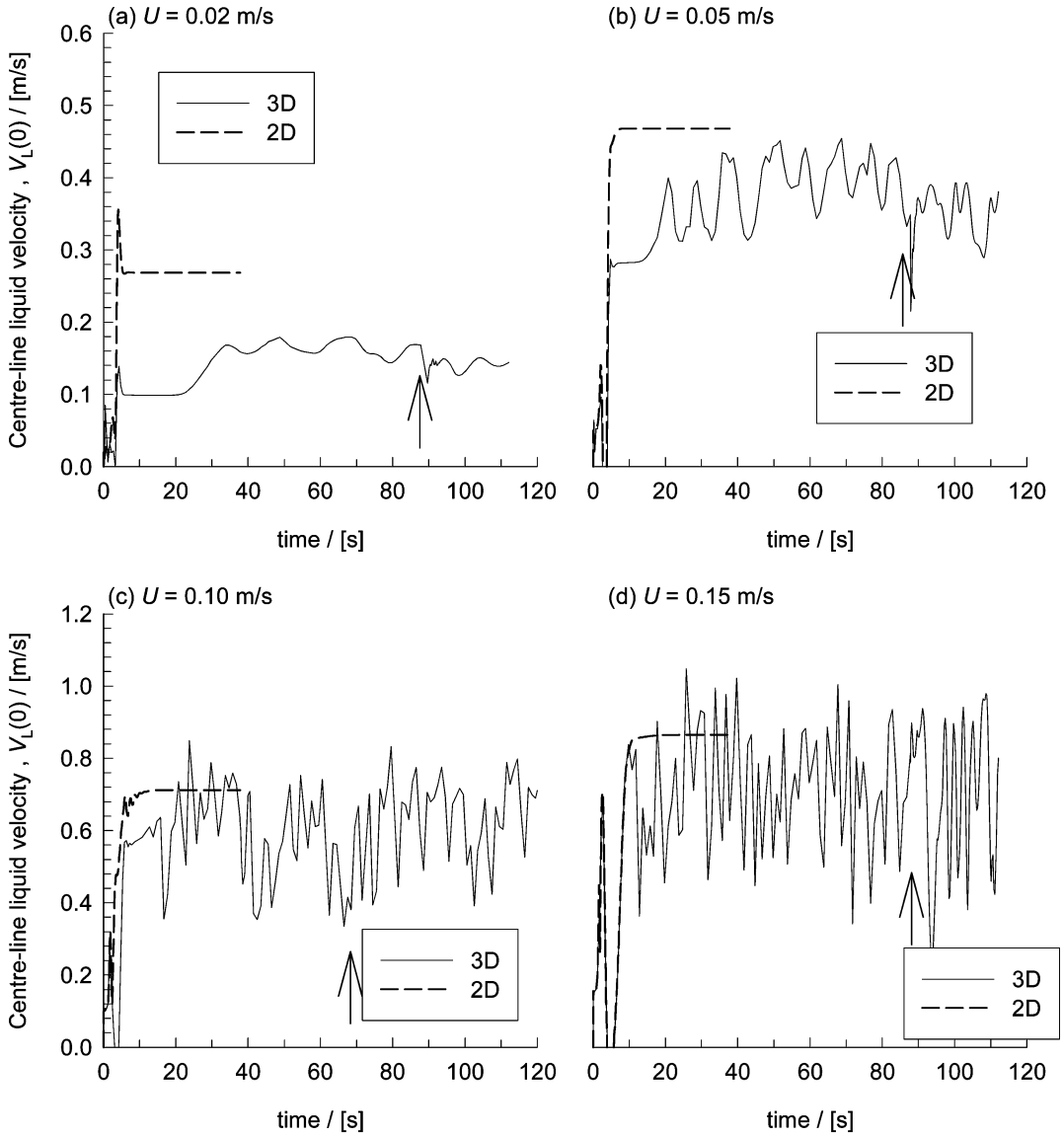

Figure 5. Transient approach to steady state (2D) or quasi-steady state (3D) for 0.38-m-diameter column, operating at U = 0.02, 0.05, 0.1, and 0.15 m/s. Comparison of 2D axisymmetric and 3D simulation strategies. The arrows represent the time of injection of tracer in 3D simulations for determination of the liquid-phase dispersion coefficient. Animations of column start-up dynamics are available on our Web site http://ct-cr4.chem.uva.nl/viscousbc/.

Here, L is the total height of the dispersion, t is the time, and L_1 and L_2 are the distances from the point of tracer injection along the dispersion height to the two monitoring stations (see Figure 3). An upper limit of n = 20 rather than infinity was found to be sufficiently accurate for the summation. The reference concentration $C_{L,0}$ was determined by the average concentration of all observation points at the end of the RTD simulation.

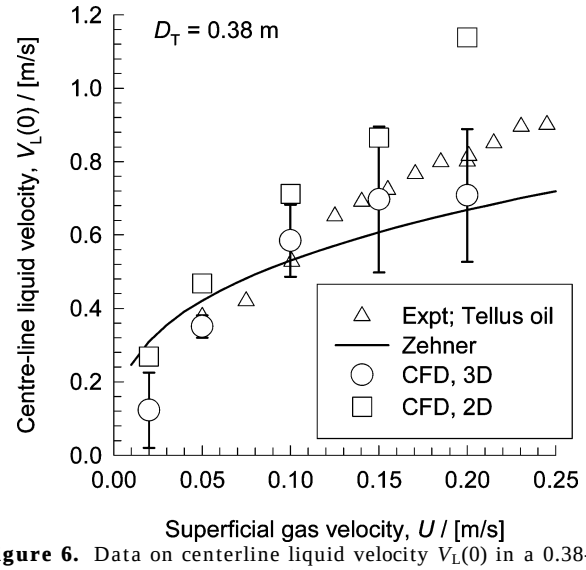

Figure 6. Data on centerline liquid velocity $V_L(0)$ in a 0.38-m-diameter column as function of U. The experimental data with Tellus oil[17] are compared with both 2D and 3D simulations. The error bars on the 3D simulation data represent the standard deviations of the transient $V_L(0)$ data presented in Figure 5, obtained from the data set after the time indicated by the arrow.

All simulations were carried out on a set of five PC Linux workstations, each equipped with a single Pentium 4 processor. The approximate times required to complete the hydrodynamic and the RTD runs are shown in Table 2. For example, a single 3D campaign at $U = 0.15$ m/s on the 10-m-diameter column took more than 2 months to produce the hydrodynamics and RTD information. Further details of the simulations, including animations of the column start-up dynamics, are available on our Web sites: http://ct-cr4.chem.uva.nl/viscousbc/ and http://ct-cr4.chem.uva.nl/FTscaleup/.

3. Results and Discussion

In Figure 4, the 2D simulations for the gas hold-up ϵ are compared with the experimental data[5] for and air−36% paraffin oil slurry system. The 2D simulations are in reasonable agreement with the experimental results for all three column diameters, 0.1, 0.19, and 0.38 m, verifying the choice of the value of $^3/_4(C_D/d_b)\rho_L$ that was calculated taking the value of $V_{b0} = 0.47$ m/s, following Figure 1c and eq 7. For the 0.38-m-diameter column, we note that the 2D and 3D simulation results are close to each other for $U = 0.02$, 0.05, and 0.1 m/s. For $U = 0.15$ m/s, the ϵ value predicted by the 3D simulation is slightly higher than that of the 2D approach. To understand the reason behind this, let us compare the dynamic behavior of the centerline liquid velocity $V_L(0)$ for the 2D and 3D strategies as it approaches a steady state; see Figure 5. The 3D simulations portray inher-

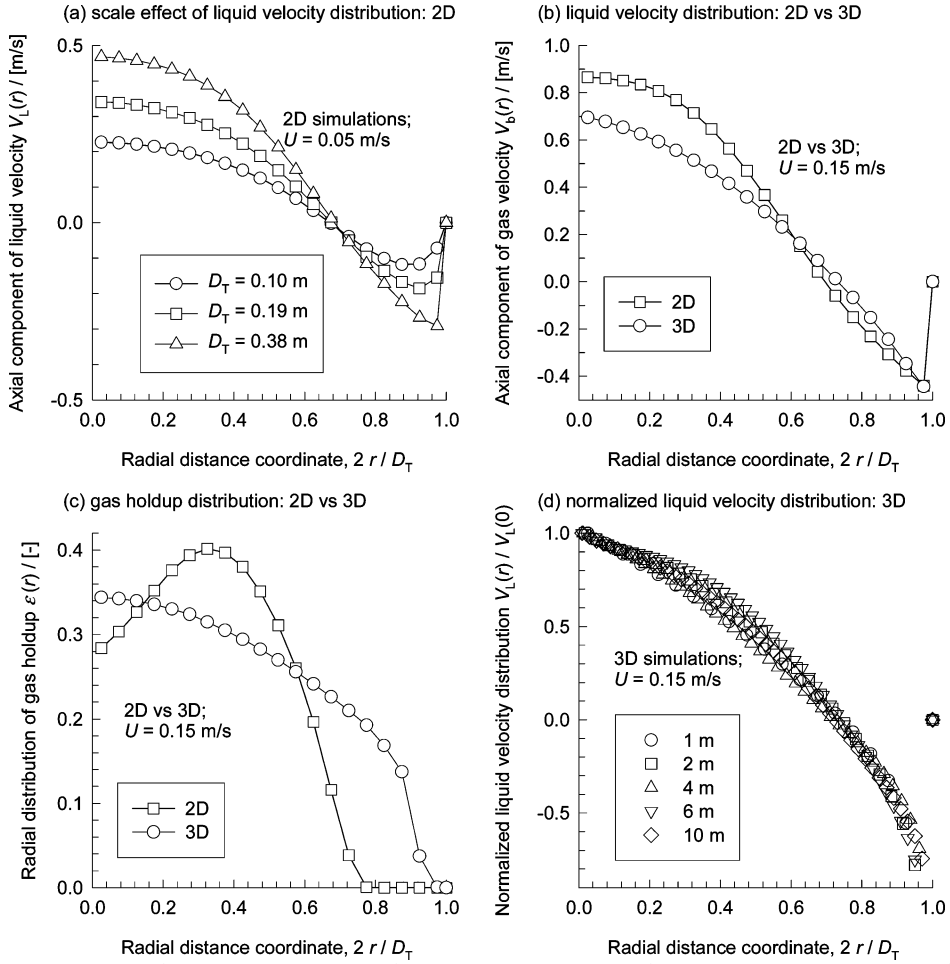

Figure 7. (a) Radial distribution of the axial component of the liquid velocity $V_L(r)$ for operation at $U = 0.05$ m/s from 2D simulations of 0.1-, 0.19-, and 0.38-m-diameter columns. (b) Comparison of 2D and 3D simulations of the radial distribution of the axial component of liquid velocity $V_L(r)$ for operation at $U = 0.15$ m/s in a 0.38-m-diameter column. (b). Comparison of 2D and 3D simulations of the radial distribution of the gas hold-up $\epsilon(r)$ for operation at $U = 0.15$ m/s in a 0.38-m-diameter column. (d) Radial distribution of the normalized axial component of liquid velocity $V_L(r)/V_L(0)$ for operation at $U = 0.15$ m/s from 3D simulations of 1-, 2-, 4-, 6-, and 10-m-diameter columns.

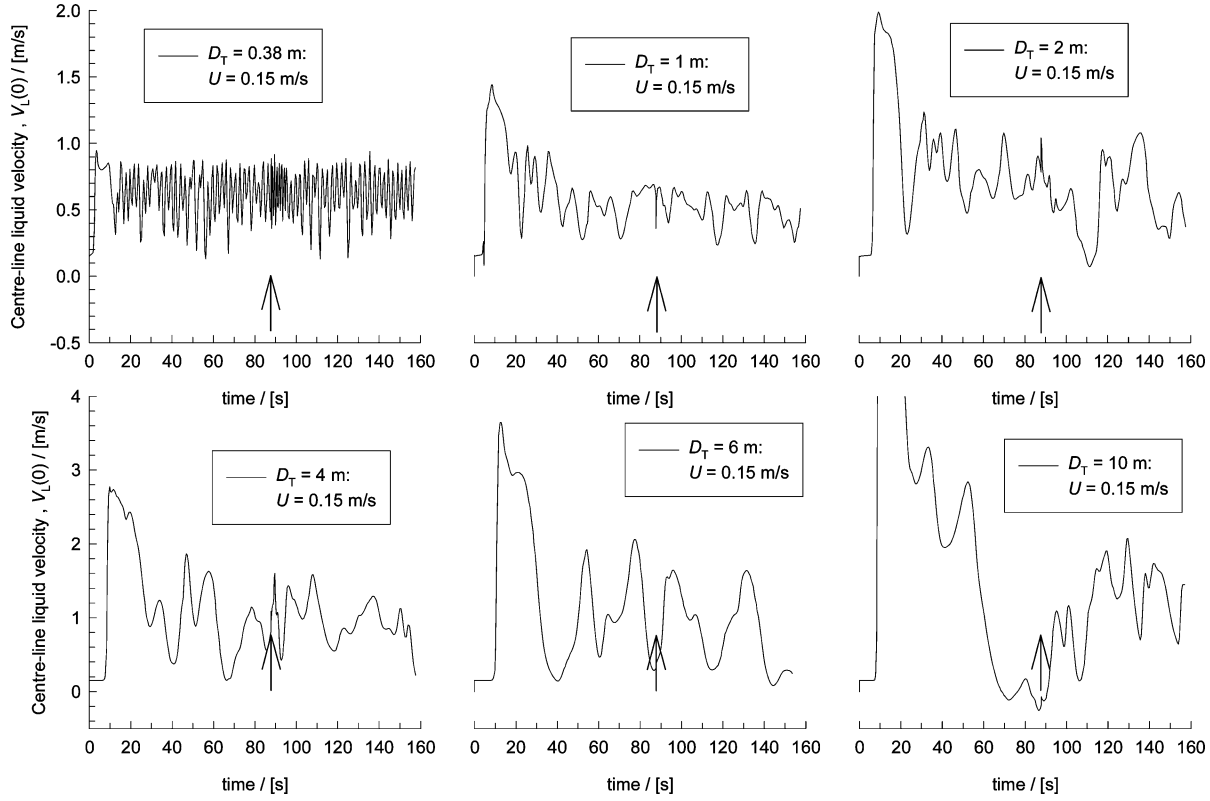

Figure 8. Transient approach to quasi-steady state (3D) for operation at $U = 0.15$ m/s in columns of 0.38-, 1-, 2-, 4-, 6-, and 10-m diameters. The arrows represent the time of injection of the tracer in 3D simulations for determination of the liquid-phase dispersion coefficient. Animations of the column start-up dynamics are available on our Web site http://ct-cr4.chem.uva.nl/FTscaleup/.

ently chaotic behavior, with liquid sloshing from side to side; these effects, which are in conformity with visual observations, can best be appreciated by viewing the animations on our Web site http://ct-cr4.chem.uva.nl/viscousbc/. The 3D simulations were run for a sufficiently long period of time, and the hydrodynamic parameters such as ϵ and $V_L(0)$ were determined by averaging over the time period where quasi-steady state prevails. The 2D simulations, on the other hand, reach a constant steady state. The time-average value of $V_L(0)$ for the 3D simulations generally tends to be lower than the corresponding value for the 2D approach; see Figure 6. The error bars for $V_L(0)$ in the 3D simulations shown in Figure 6 represent the standard deviations obtained from the transient $V_L(0)$ dynamics in Figure 5. We also note from Figure 6 that the differences in the 2D and 3D simulation results increase with increasing U. The experimental data[17] for $V_L(0)$ for an air−Tellus oil system are in better agreement with the 3D simulation results, emphasizing the superiority of the 3D approach.

Figure 7a shows the radial distribution of the axial component of the liquid velocity, $V_L(r)$, obtained from 2D simulations for $D_T = 0.1$, 0.19, and 0.38 m and $U = 0.05$ m/s. We see that the liquid circulation velocities increase strongly with column diameter. At the center of the column, for example, the axial component of the liquid velocity $V_L(0)$ is 0.23 m/s in the 0.1-m-diameter column; this value increases to 0.34 m/s in the 0.19-m-diameter column and to 0.47 m/s in the 0.38-m-diameter column. Because the drag coefficient between the gas bubbles and the liquid is the same for all column diameters, the rise velocity of the bubbles has to increase with increasing column diameter. Figure 7b compares the $V_L(r)$ profile from 2D and 3D simulations for $U = 0.15$ m/s and $D_T = 0.38$ m. As was remarked earlier in the context of Figure 6, the 3D simulations predict a more realistic value of $V_L(0)$ in accord with experimental data.[29] The shortcomings of the 2D simulation strategy become more apparent when we consider the radial distribution of the gas hold-up, $\epsilon(r)$. The predictions of the 2D and 3D simulations of $\epsilon(r)$ for $U = 0.15$ m/s and $D_T = 0.38$ m are compared in Figure 7c. The 2D simulations predict an unrealistic off-center maximum in the gas hold-up, whereas the 3D simulations yield the classical parabolic hold-up profile, often observed in practice.[8,29,30] The average gas hold-ups, ϵ, however, for the 2D and 3D simulations are very close to each other.

For the FT slurry reactor, the optimum operating value of U is in the range of 0.2−0.3 m/s, as discussed by Maretto and Krishna.[3] However, because syngas is being consumed to form liquid product, the value of U at the outlet of the reactor is only 30−40% of the inlet value, depending on the conversion level. For an FT reactor operating at a value of $U = 0.25$ m/s at the bottom, the value of U at the top of the reactor will be reduced to about 0.10 m/s. Therefore, in our simulations for the FT reactor hydrodynamics as a function of scale (for column diameters $D_T = 0.38$, 1, 2, 4, 6, and 10 m; also see Table 2 for column heights used), we chose to perform transient 3D simulations at $U = 0.15$ m/s, an average value between 0.1 and 0.25 m/s. The transient dynamics of the centerline velocity (monitored at the observation heights, H_{obs}, specified in Table 2) are shown in Figure 8. It is apparent that, with increasing scale, both the magnitude of $V_L(0)$ and its fluctuation around the mean increases. The hydrodynamic parameters obtained by averaging over the time period during which quasi-steady state can be assumed to prevail. These time-averaged values of $V_L(0)$ are shown in Figure 9a, in which the error bars represent the standard

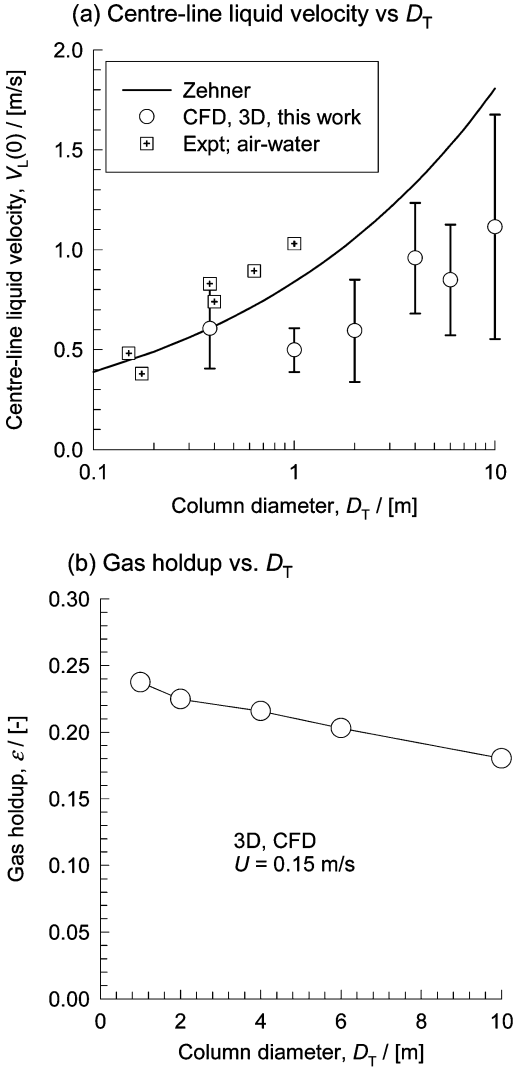

Figure 9. 3D simulation data on (a) centerline liquid velocity $V_L(0)$ and (b) gas hold-up ϵ as functions of D_T for operation at $U =$ 0.15 m/s in columns of 0.38-, 1-, 2-, 4-, 6-, and 10-m diameters. The error bars on the 3D simulation data in a represent the standard deviations of the transient $V_L(0)$ data presented in Figure 8, obtained from the data set after the time indicated by the arrow mark. The continuous line in a represents the correlation of Zehner.[13] Also plotted in a are the experimental data of Forret et al.[8] and Krishna et al.[11]

deviations of the velocity fluctuations shown in Figure 8. The $V_L(0)$ values, which increase with scale, appear to follow the trend predicted by the Zehner correlation,[13] but the absolute values are significantly lower. Earlier work using 2D axisymmetric simulations for scaling up bubble column reactors[4] had predicted $V_L(0)$ values conforming with the correlation of Riquarts[12] and significantly higher than found in the present study with realistic 3D simulations. The $V_L(0)$ predictions of this earlier work[4] are unrealistically high because of the artifacts introduced in the 2D approach as explained in the foregoing discussion.

When compared with the air−water experimental data[8,11] for $V_L(0)$, we see that the CFD predictions for the FT reactor are significantly lower, stressing the danger of using air−water information for scaling up other systems. The main reason for the lower $V_L(0)$ predicted for the FT reactor is the significantly lower gas hold-up when compared to air−water systems. For air−water systems, operating at $U = 0.15$ m/s, a significant fraction of the dispersion would be present in the form of small bubbles; this small bubble population is virtually destroyed in concentrated slurries,[31] leading to significantly lower gas hold-ups and $V_L(0)$ values.

When the liquid velocity profiles obtained from the 3D CFD simulations are normalized with respect to the centerline velocity, the $V_L(r)/V_L(0)$ values are practically independent of the column diameter. This is illustrated in Figure 7d for the 3D simulation campaign at $U =$ 0.15 m/s for various column diameters up to 10 m. The significance of the result portrayed in Figure 7d is that the centerline velocity can be taken to be a unique measure of the strength of liquid circulation.

An important consequence of the fact that the strength of the liquid circulation increases with increasing scale is that the gas hold-up values are correspondingly lowered; this is shown in Figure 9b. We note that the gas hold-up in the 10-m-diameter FT reactor is 0.18, whereas for the 1-m-diameter column, the value of ϵ is 0.24. A 20% decrease in gas hold-up with increase in scale can have significant consequences for an FT reactor designed for high conversion targets.

A tracer is injected into the liquid phase near the top of the liquid dispersion at the time step indicated by an arrow in Figure 8, and the progression of this tracer is monitored at two stations along the height of the column (see Figure 3). The CFD simulations of the tracer RTD are then fitted with the model given by eq 9. A comparison of typical results for the dimensionless RTD curves for the tracer is shown in Figure 10 for columns with (a) $D_T = 0.38$ m and (b) $D_T = 2$ m, both operating at $U = 0.15$ m/s. We note from Figure 10 that the tracer response is not smooth but oscillates. These oscillations are due to liquid sloshing from side to side causing a significant radial transport of the liquid tracer, as can be witnessed in the animations on our Web site http://ct-cr4.chem.uva.nl/FTscaleup/. In this context, it is worth emphasizing that 2D simulations will yield a much lower value of $D_{ax,L}$ than 3D simulations because there is no mechanism for radial transport in the former.[10]

Each of the tracer curves, such as those shown in Figure 10, was fitted individually to obtain two different values of $D_{ax,L}$ for each run. Figure 11 shows the results for the two campaigns with (a) varying U for $D_T = 0.38$ m and (b) varying D_T for $U = 0.15$ m/s. Also plotted in Figure 11 are the experimentally determined $D_{ax,L}$ values for the air−water system.[8,17] The $D_{ax,L}$ values from our 3D simulations are lower than the experimental values for the air−water system, following the same trend as observed earlier for the $V_L(0)$ values in Figure 9a. The $V_L(0)$ value reflects the strength of liquid circulation, and this circulation directly influences liquid dispersion. The predictions for $D_{ax,L}$ using the Baird−Rice correlation[18] (shown by the continuous lines in Figure 11), though representing the air−water data reasonably accurately, tend to be higher than the values for the FT reactor operating with a concentrated oil slurry. We note that the simulated value of $D_{ax,L}$ for the 10-m-diameter reactor is expected to lie between 3 and 7 m^2/s, corresponding to a nearly well-mixed system.

Another important design parameter is the coefficient for heat transfer to the vertical cooling tubes, α; this parameter is largely dictated by the surface renewal rate, which, in turn, is determined by the bubble rise velocity. Increased liquid circulation velocities with increasing scale will have the effect of enhancing the bubble rise velocity and improving the heat-transfer coefficients. Therefore, CFD predictions of $V_L(0)$ with

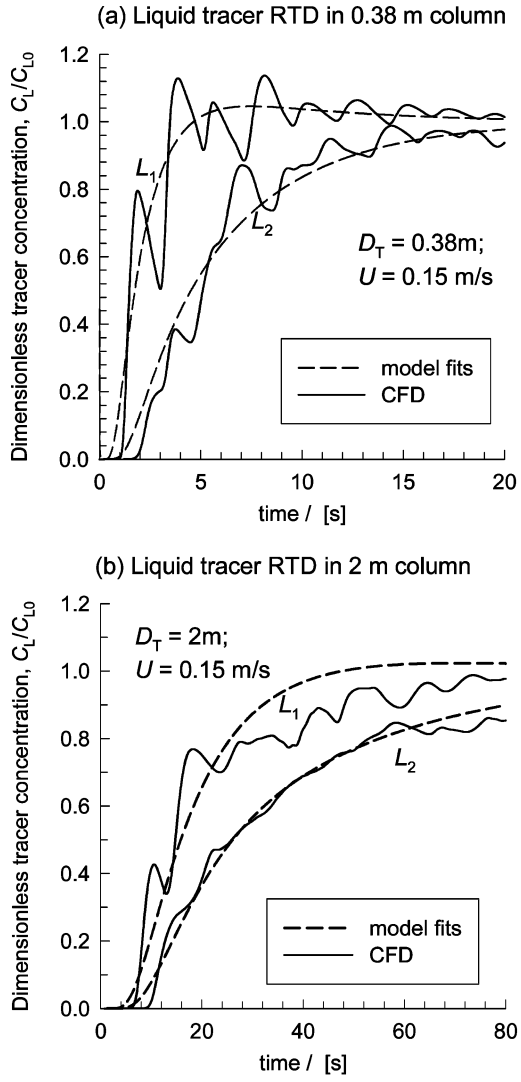

Figure 10. 3D simulations of the dimensionless liquid tracer concentration measured at two different monitoring stations for (a) a 0.38-m-diameter column operating at $U = 0.15$ m/s and (b) a 2-m-diameter column operating at $U = 0.15$ m/s. The dashed lines represent the fits of the two simulation data sets using eq 9. Animations of liquid tracer dynamics are available on our Web site http://ct-cr4.chem.uva.nl/FTscaleup/.

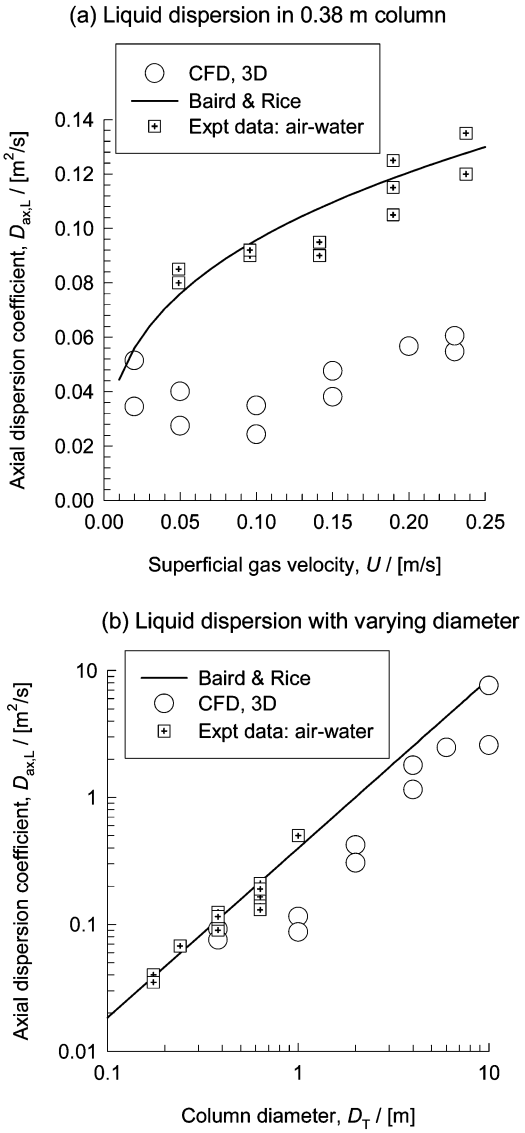

Figure 11. (a) Liquid-phase axial dispersion ($D_{ax,L}$) data obtained from 3D simulations of a 0.38-m-diameter column operating at $U = 0.02-0.23$ m/s. (b) $D_{ax,L}$ data from 3D simulations for operation at $U = 0.15$ m/s in columns of 0.38-, 1-, 2-, 4-, 6-, and 10-m diameters. Note that the data for the 0.38-m-diameter column in b were obtained at a higher aspect ratio than for the simulations for the same column shown in a; details are given in Table 2. The continuous lines in a and b represent the correlation of Baird and Rice.[18] Also plotted in b are the experimental data for $D_{ax,L}$ of Forret et al.[8] and Krishna et al.[17]

scale allow for better estimation of the heat-transfer coefficient to the vertical cooling tubes.[32]

4. Conclusions

In this paper, we have advocated the use of Eulerian simulations for obtaining information on the hydrodynamics of FT slurry reactors in columns with diameters ranging from 1 to 10 m. The crucially important inputs concerning the drag coefficient C_D and the bubble diameter were estimated from measurement data with a 36 vol % slurry in columns of relatively small scale, 0.1−0.38 m in diameter, on the bubble swarm velocity at vanishingly small U values.

The following major conclusions can be drawn from this work:

(1) Both 2D and 3D simulations are able to provide a reasonable prediction of the *average* gas hold-up ϵ for columns with diameters of 0.1, 0.19, and 0.38 m.

(2) The 2D simulations generally tend to predict a higher value of $V_L(0)$ than the 3D simulations. For very large diameter columns, the 2D predictions of $V_L(0)$ are unrealistically high.[4] For scaling up to columns larger than 1 m in diameter, it is essential to resort to 3D simulations.

(3) The 2D predictions of the radial distribution of the gas hold-up $\epsilon(r)$ show an unrealistic off-center maximum in the gas hold-up. The 3D simulations of $\epsilon(r)$ yield the classical parabolic profile typically found in experiments.

(4) For larger-diameter columns, only 3D simulations are able to reproduce the chaotic hydrodynamics observed visually, and only this strategy can yield reasonable values of $V_L(0)$ and $D_{ax,L}$ for large-diameter FT reactors. 2D simulations of $D_{ax,L}$ give unrealistically low values because the radial dispersion contribution is absent.[10]

(5) 3D simulations of FT reactor with diameters of 0.38, 1, 2, 4, 6 and 10 m show that the $V_L(0)$ values are

lower than those predicted by the Zehner correlation,[13] which is apparently adequate only for describing the air−water system.

(6) The axial dispersion coefficient of the liquid phase, $D_{ax,L}$, for the FT reactor shows a trend similar to that for $V_L(0)$; the values are lower than those obtained for air−water experiments. The predictions of $D_{ax,L}$ following the Baird and Rice correlation[18] tend to yield somewhat higher values than those obtained from CFD simulations.

We conclude that 3D Eulerian simulations can provide a powerful tool for hydrodynamic scale-up of bubble columns, obviating the need for large-scale experiments on gas hold-up, liquid velocity, and mixing. Validation of the proposed scale-up strategy, however, is desirable, provided that experiments can be carried out in columns larger than, say, 2 m in diameter operating with an oil slurry.

Acknowledgment

The Netherlands Organization for Scientific Research (NWO) is gratefully acknowledged for providing financial assistance in the form of a "programmasubsidie" for development of novel concepts in reactive separations technology.

Nomenclature

a = interfacial area per unit volume of dispersion, $m^2\ m^{-3}$
C_D = drag coefficient
C_L = liquid-phase concentration, arbitrary units
d_b = bubble diameter, m
$\mathscr{D}_k$ = diffusivity in phase k, $m^2\ s^{-1}$
$D_{ax,L}$ = liquid-phase axial dispersion coefficient, $m^2\ s^{-1}$
D_T = column diameter, m
$\mathbf{g}$ = gravitational vector, $m\ s^{-2}$
H_0 = initial height of liquid in the column, m
H_{obs} = height at which the simulations are monitored (observed), m
H_T = total reactor height, m
k_L = mass-transfer coefficient, m/s
L_i = distance between tracer injection and monitoring, m
$\mathbf{M}$ = interphase momentum-exchange term, N/m^3
n = index used in eq 9
p = system pressure, Pa
r = radial coordinate, m
t = time, s
T = temperature, K
$\mathbf{u}$ = velocity vector, m/s
U = superficial gas velocity, $m\ s^{-1}$
V_b = bubble swarm velocity, $m\ s^{-1}$
V_{b0} = bubble swarm velocity extrapolated to zero gas velocity, $m\ s^{-1}$
$V_L(r)$ = radial distribution of liquid velocity, $m\ s^{-1}$
$V_L(0)$ = centerline liquid velocity, $m\ s^{-1}$

Greek Letters

α = heat-transfer coefficient, $W\ m^{-2}\ K^{-1}$
ϵ = total gas hold-up
$\epsilon(r)$ = radial gas hold-up profile
ϵ_s = solids hold-up
ϵ_k = hold-up of phase k
μ = viscosity of the fluid phase, Pa s
ρ = density of phase, $kg\ m^{-3}$
σ = surface tension of the liquid phase, $N\ m^{-1}$

Subscripts

eff = effective
G = referring to gas
L = referring to liquid
k, l = referring to phases k and l, respectively
s = solids
T = tower or column

Literature Cited

(1) Sie, S. T.; Krishna, R. Fundamentals and selection of advanced Fischer−Tropsch reactors. *Appl. Catal. A: Gen.* **1999**, *186*, 55.

(2) Krishna, R.; Sie, S. T. Design and scale-up of the Fischer−Tropsch bubble column slurry reactor. *Fuel Process. Technol.* **2000**, *64*, 73.

(3) Maretto, C.; Krishna, R. Modelling of a bubble column slurry reactor for Fischer−Tropsch synthesis, *Catal. Today* **1999**, *52*, 279.

(4) Krishna, R. A scale-up strategy for a commercial scale bubble column slurry reactor for Fischer−Tropsch synthesis. *Oil Gas Sci. Technol.* **2000**, *55*, 359.

(5) Krishna, R.; Urseanu, M. I.; de Swart, J. W. A.; Ellenberger, J. Gas hold-up in bubble columns: Operation with concentrated slurries versus high viscosity liquid. *Can. J. Chem. Eng.* **2000**, *78*, 442.

(6) Urseanu, M. I.; Guit, R. P. M.; Stankiewicz, A.; van Kranenburg, G.; Lommen, J. Influence of operating pressure on the gas hold-up in bubble columns for high viscous media. *Chem. Eng. Sci.* **2003**, *58*, 697.

(7) Krishna, R.; van Baten, J. M. Scaling up bubble column reactors with highly viscous liquid phase. *Chem. Eng. Technol.* **2002**, *25*, 1015.

(8) Forret, A.; Schweitzer, J.-M.; Gauthier, T.; Krishna, R.; Schweich, D. Influence of scale on the hydrodynamics of bubble column reactors: An experimental study in columns of 0.1, 0.4 and 1 m diameters. *Chem. Eng. Sci.* **2003**, *58*, 719.

(9) Wilkinson, P. M.; Spek, A. P.; Van Dierendonck, L. L. Design Parameters Estimation for Scale-up of High-Pressure Bubble-Columns. *AIChE J.* **1992**, *38*, 544.

(10) van Baten, J. M.; Krishna, R. Eulerian simulations for determination of the axial dispersion of liquid and gas phases in bubble columns operating in the churn-turbulent regime. *Chem. Eng. Sci.* **2001**, *56*, 503.

(11) Krishna, R.; Urseanu, M. I.; van Baten, J. M.; Ellenberger, J. Influence of scale on the hydrodynamics of bubble columns operating in the churn-turbulent regime: Experiments vs Eulerian simulations. *Chem. Eng. Sci.* **1999**, *54*, 4903.

(12) Riquarts, H. P. Strömungsprofile, Impulsaustausch und Durchmischung der flüssigen Phase in Bläsensaulen. *Chem. Ing. Tech.* **1981**, *53*, 60.

(13) Zehner, P. Momentum, mass and heat transfer in bubble columns. Part 1. Flow model of the bubble column and liquid velocities. *Int. Chem. Eng.* **1986**, *26*, 22.

(14) Koide, K.; Morooka, S.; Ueyama, K.; Matsuura, A.; Yamashita, F.; Iwamoto, S.; Kato, Y.; Inoue, H.; Shigeta, M.; Suzuki, S.; Akehata, T. Behaviour of bubbles in large scale bubble column. *J. Chem. Eng. Jpn.* **1979**, *12*, 98.

(15) Kojima, E.; Unno, H.; Sato, Y.; Chida, T.; Imai, H.; Endo, K.; Inoue, I.; Kobayashi, J.; Kaji, H.; Nakanishi, H.; Yamamoto, K. Liquid-phase velocity in a 5.5 m diameter bubble column. *J. Chem. Eng. Jpn.* **1980**, *13*, 16.

(16) Maretto, C.; Krishna, R. Design and optimisation of a multi-stage bubble column slurry reactor for Fischer−Tropsch synthesis. *Catal. Today* **2001**, *66*, 241.

(17) Krishna, R.; Urseanu, M. I.; van Baten, J. M.; Ellenberger, J. Liquid-phase dispersion in bubble columns operating in the churn-turbulent flow regime. *Chem. Eng. J.* **2000**, *78*, 43.

(18) Baird, M. H. I.; Rice, R. G. Axial dispersion in large unbaffled columns, *Chem. Eng. J.* **1975**, *9*, 171.

(19) Wilkinson, P. M.; Haringa, H.; Stokman, F. P. A.; Van Dierendonck, L. L. Liquid-Mixing in a Bubble Column under Pressure. *Chem. Eng. Sci.* **1993**, *48*, 1785.

(20) Yang, G. Q.; Fan, L. S. Axial liquid mixing in high-pressure bubble columns. *AIChE J.* **2003**, *49*, 1995.

(21) Pan, Y.; Dudukovic, M. P.; Chang, M. Dynamic simulation of bubbly flow in bubble columns. *Chem. Eng. Sci.* **1999**, *54*, 2481.

(22) Sanyal, J.; Vasquez, S.; Roy, S.; Dudukovic, M. P. Numerical simulation of gas−liquid dynamics in cylindrical bubble column reactors. *Chem. Eng. Sci.* **1999**, *54*, 5071.

(23) Sokolichin, A.; Eigenberger, G. Applicability of the standard k-epsilon turbulence model to the dynamic simulation of

bubble columns: Part I. Detailed numerical simulations. *Chem. Eng. Sci.* **1999**, *54*, 2273.

(24) Clift, R.; Grace, J. R.; Weber, M. E. *Bubbles, Drops and Particles*; Academic Press: San Diego, CA, 1978.

(25) Vandu, C. O.; Krishna, R. Gas holdup and volumetric mass transfer coefficient in a slurry bubble column. *Chem. Eng. Technol.* **2003**, *26*, 779.

(26) Rhie, C. M.; Chow, W. L. Numerical study of the turbulent flow past an airfoil with trailing edge separation. *AIAA J.* **1983**, *21*, 1525.

(27) van Doormal, J.; Raithby, G. D. Enhancement of the SIMPLE method for predicting incompressible flows. *Numer. Heat Transfer* **1984**, *7*, 147.

(28) Deckwer, W. D. *Bubble Column Reactors*; John Wiley: New York, 1992.

(29) Krishna, R.; van Baten, J. M.; Urseanu, M. I. Three-phase Eulerian simulations of bubble column reactors operating in the churn-turbulent regime: A scale-up strategy. *Chem. Eng. Sci.* **2000**, *55*, 3275.

(30) Kemoun, A.; Ong, B. C.; Gupta, P.; Al-Dahhan, M. H.; Dudukovic, M. P. Gas holdup in bubble columns at elevated pressure via computed tomography. *Int. J. Multiphase Flow* **2001**, *27*, 929.

(31) De Swart, J. W. A.; van Vliet, R. E.; Krishna, R. Size, structure and dynamics of "large" bubbles in a two- dimensional slurry bubble column. *Chem. Eng. Sci.* **1996**, *51*, 4619.

(32) Yang, G. Q.; Luo, X.; Lau, R.; Fan, L. S. Heat Transfer Characteristics in Slurry Bubble Columns at Elevated Pressures and Temperatures. *Ind. Eng. Chem. Res.* **2000**, *39*, 2568.

Received for review July 29, 2003
Revised manuscript received September 11, 2003
Accepted September 16, 2003

IE0340286